

Chapter 9

Study of Residual Stress in Nickel Micro Parts Made by Electrochemical Additive Manufacturing



Anne Brant, Abishek Kamaraj and Murali Sundaram

Abstract Electrochemical additive manufacturing (ECAM) is a novel process which uses localized electrochemical deposition as the material addition mechanism for additive manufacturing (AM) of metal parts at room temperature. While ECAM possesses highly controllable process parameters, complex electrochemical phenomena, such as nucleation patterns and hydrogen codeposition, may cause residual stresses in the output parts. To better predict this behavior for increased reliability and future commercial adoption of ECAM, localized deposits were studied under several controlled combinations of electrochemical process parameters under both constant-time and constant-height termination criteria. The residual stress was then measured using an atomic force microscopy (AFM) indentation procedure. Significant trends that were found include increased stress magnitude with increasing applied voltage, and the higher influence of voltage and then pulse period on the resulting stress, compared to the duty cycle. It was also seen that shorter deposition times led to compressive stresses and longer times led to tensile stresses.

Keywords Additive manufacturing · Electrodeposition · Residual stress

9.1 Introduction

Additive manufacturing (AM) methods are increasingly being used to manufacture functional parts. A significant amount of applications are present in the biomedical and aerospace industries, where highly customized parts are needed. However, the lack of industry confidence in the material properties of the parts curbs the widespread use of these processes. While some AM processes such as selective laser melting and electron beam melting are capable of producing parts on par with or even superior to conventionally machined ones, they suffer from very high residual stresses due to the complete melting of the material during manufacturing [1]. Also, traditional AM techniques have limitations such as choice of material, anisotropy, porosity, strength,

A. Brant · A. Kamaraj · M. Sundaram (✉)
University of Cincinnati, Cincinnati, OH 45221, USA
e-mail: murali.sundaram@uc.edu

© Springer Nature Singapore Pte Ltd. 2020
M. S. Shunmugam and M. Kanthababu (eds.), *Advances in Additive Manufacturing and Joining*, Lecture Notes on Multidisciplinary Industrial Engineering,
https://doi.org/10.1007/978-981-32-9433-2_9

scalability, support structure, thermal defects, and internal stresses. For example, high residual stresses (>200 MPa) are caused by the thermal gradient associated with sintering processes. Thus, even though AM processes are capable of producing any design, the residual stresses impart constraints on the wall thickness of the parts that are being produced.

Electrochemical additive manufacturing (ECAM) is a novel additive manufacturing process, which can manufacture 3D metal parts at room temperature directly from 3D model files. ECAM combines the principles of localized electrochemical deposition (LECD) with the layer-by-layer manufacturing procedure of additive manufacturing to create parts directly from 3D CAD models [2]. The ECAM process flow is illustrated as a schematic in Fig. 9.1.

LECD is capable of depositing most conductive materials, including metals, metal alloys, conducting polymers, and even some semiconductors [4]. It is a process of material addition that is electrochemical in nature (atom-by-atom); thus, the properties of the deposited materials can be modified as desired by varying the specific process parameters shown to yield the desired result. The residual stresses associated with the pulsed electrodeposition and electroforming processes are expected to be negligible as compared to those of sintering and melting processes. However, LECD is not totally a stress-free additive manufacturing process.

For example, electrochemical co-deposition of metal hydrides along with the metal is known to cause residual stresses during the electrodeposition process [5]. These stresses cause the deposited material to distort, which is especially pronounced in the case of micro components. Another cause for residual stresses in electrodeposits is from the mechanism of nucleation and growth of grains resulting in stresses

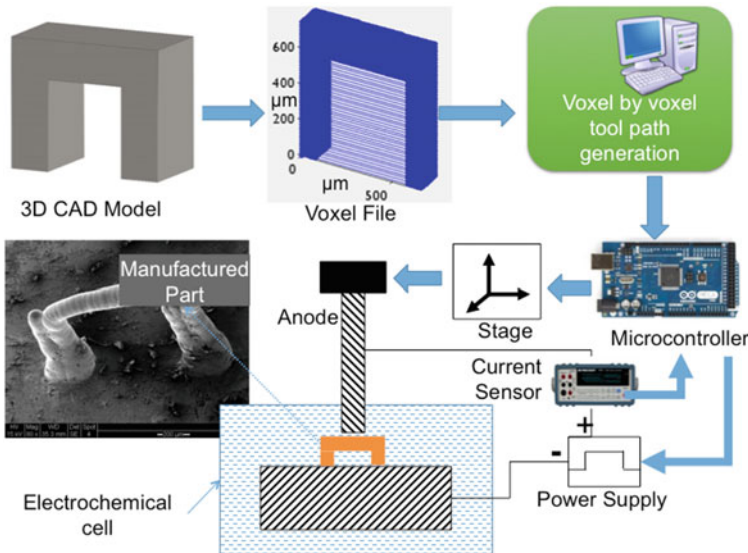


Fig. 9.1 Illustration of the steps involved in the electrochemical additive manufacturing [3]

both compressive and tensile. Both these mechanisms offer contradicting effects of current density on the internal stresses. While in some cases, higher current density increases the stresses [5], in others, the opposite effect is noticed [6].

Despite these considerations, ECAM still possesses advantages over related processes. For example, micro-electroformed parts are prone to local residual stress gradients. Prior work shows this can be mitigated by pre-setting a stress-release geometry [7]. However, this requires extra work and analysis that must be performed for each geometry, which would add to time, cost, and labor in manufacturing. Additionally, there could be a risk of damage and inconsistency in the part due to the stress release process. In contrast, ECAM allows for locally controllable electrochemical parameters that then give controllable residual stress at the local level for micro parts.

Compared to these other processes, the ECAM process has a significant versatility in local control of input and output parameters, including residual stress. It is therefore highly valuable to gain an understanding of the relationships between input and output parameters. Control of residual stress allows for its minimization, which results in better repeatability and reliability [8]. These are critical steps for ECAM to become a commercially viable additive manufacturing process.

In this work, the effects of varying deposition parameters using pulsed current were studied. Pulsed power during electrodeposition produces parts with higher strength when compared to parts made using DC power [9]. Input parameters included constant time versus height conditions, voltage, pulse period, and duty cycle.

9.2 Experimental Methods

9.2.1 Electrochemical Deposition

The experimental setup is given in Fig. 9.2. Watts bath was used as the electrolyte. A side-insulated platinum microelectrode and a highly polished brass metal plate were used as the anode and cathode, respectively. A pulsed power supply was used to provide square current pulses with varying levels of voltages, duty cycles, and pulse periods. Multiple trials of the deposits under each experimental condition were made to minimize the effect of experimental variations. One set of trials was performed under a constant gap condition, and another set of trials was performed at the same initial inter-electrode gap, but for constant-time conditions. All parameters are summarized in Table 9.1.

9.2.2 Residual Stress Measurement

Overview. An existing nanoindentation technique of measuring residual stresses [10] was adapted for use with the atomic force microscope (AFM) in this study.

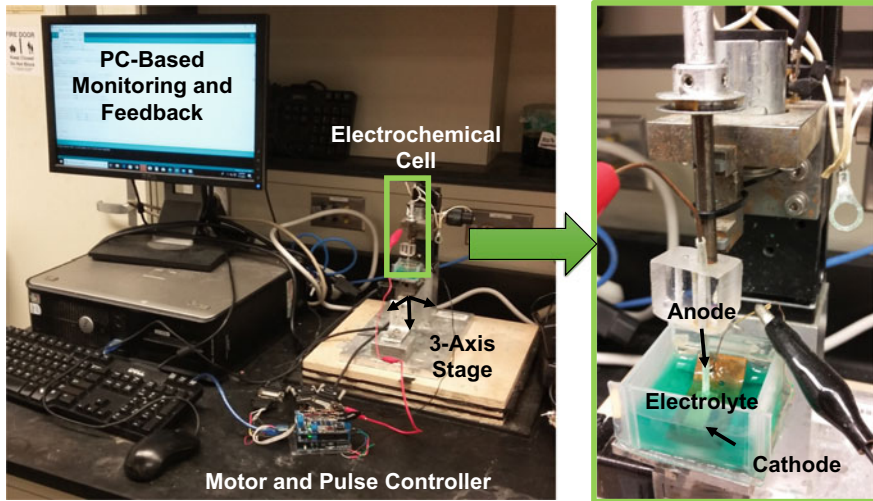


Fig. 9.2 ECAM experimental setup

Table 9.1 Levels of the experimental parameters used in this study

Process parameter	Levels
Voltage (V)	3, 4, 5
Pulse period (ns)	100, 200
Duty cycle (%)	50, 75
Initial inter-electrode gap (μm); all trials	10
Total deposition time (s); constant-time trials	30

This technique uses the retraction force-indentation curves from indentation into the parts to determine the magnitude and type (compressive or tensile) of residual stress. Figure 9.3 illustrates how the force P acts on the deposit and the indentation depth h physically observed during the AFM indentation process, and Fig. 9.3a illustrates the form of a typical force-indentation ($P-h$) curve for an AFM tip of angle 2γ . Only the retraction curve is necessary to calculate the residual stress, detailed in further equations.

Figure 9.3a also illustrates the phenomena that occur when an AFM tip of angle 2γ is indented into the sample. When the stress is tensile, as shown in Fig. 9.3b, the material is easier to indent, and the force-indentation curve is less steep than the curve of an unstressed sample of the same composition (referred to as the reference curve). When the stress is compressive, as shown in Fig. 9.3c, the material is not as easy to indent, and the force-indentation curve is steeper relative to the reference curve [10]. Furthermore, the illustrations show that the phenomena that occur at tensile and compressively stressed elements are not completely opposite. For the compressive element, the value of α corresponds to the angle between the tip of the

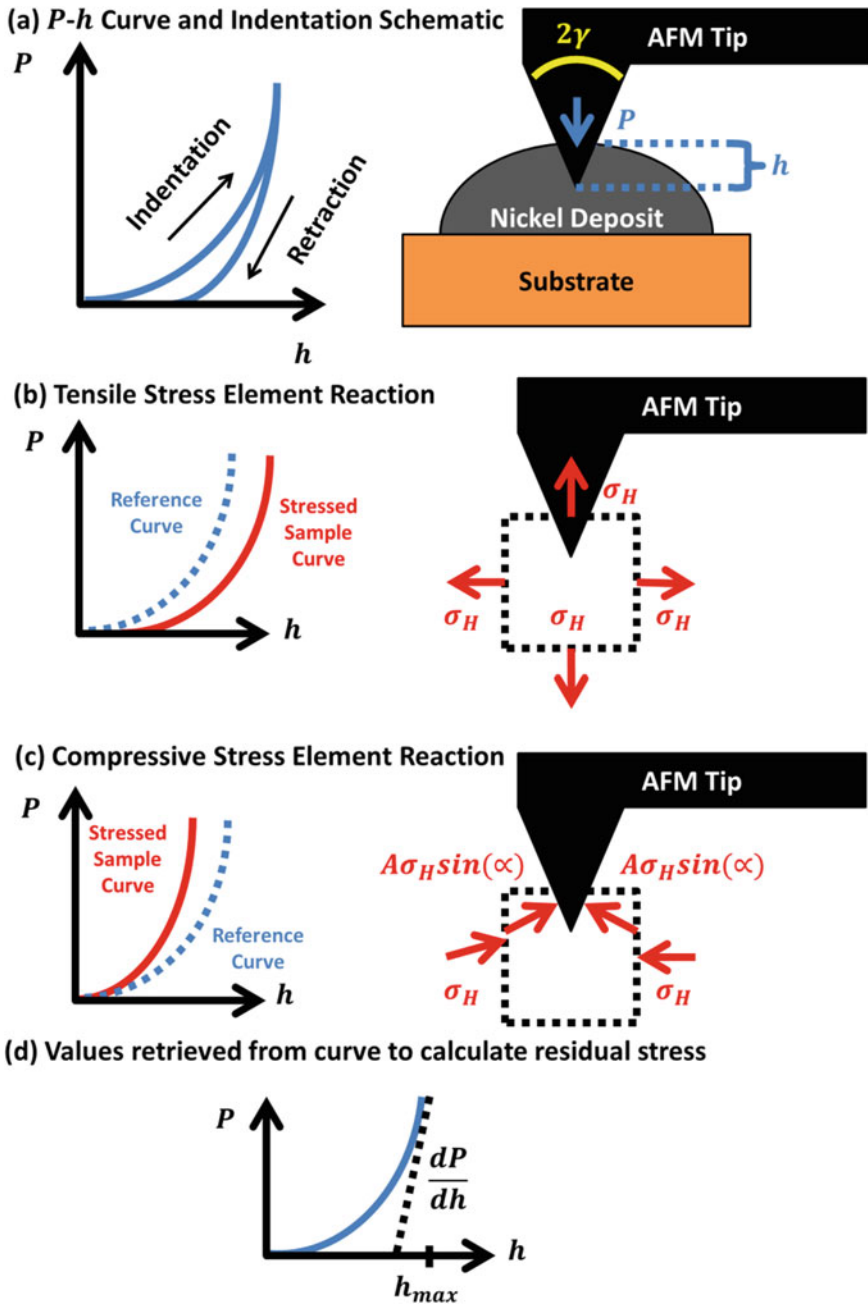


Fig. 9.3 *P-h* curve interpretation and AFM indentation mechanisms

AFM and the horizontal:

$$\alpha = \gamma - \frac{\pi}{2} \quad (9.1)$$

For small parts manufactured at the micro- and nanoscale, it is more advantageous to use the AFM instead of a conventional nanoindenter. A typical Berkovich indenter tip radius is in the range of 50–150 nm and imparts a force of the order of several mN [11], while the AFM tips used in this experiment have a tip radius between 8 and 35 nm and impart a force in a range of several μN . Because the smaller tip of the AFM imparts less force, there is less risk of damage to the small part. Also, since the electrodeposited parts are constructed atom by atom, a smaller tip gives a more accurate account of the material behavior of the part at the atomic scale.

Preparation. An AFM with contact mode and force curve plotting capability is used to measure the residual stress in the electrodeposited parts. An equivalent Young's modulus E^* is calculated from Young's modulus and Poisson's ratio for both the sample material and AFM probe [10]:

$$E^* = \left(\frac{1 - \nu^2}{E} + \frac{1 - \nu_{\text{in}}^2}{E_{\text{in}}} \right) \quad (9.2)$$

where

- ν Poisson's ratio of the substrate
- E Young's modulus of the substrate
- ν_{in} Poisson's ratio of the indenter
- E_{in} Young's modulus of the indenter

The following assumptions were used in the measurement process. They are a combination of assumptions used in experiments by Suresh and Giannakopoulos [10], as well as assumptions specific to the electrodeposition and AFM measurement.

1. The residual stress σ_{H} is equibiaxial across any given element on the surface of the measured part.
2. The stresses are uniform beneath to a depth of influence d_{R} , which is a function of A , the contact area between the indenter and the sample.
3. $d_{\text{R}} = 7\sqrt{A\pi}$ (9.3)
4. The sample is isotropic and permitted to undergo isotropic strain hardening.
5. The sample is pre-stressed from the electrodeposition process.
6. The indentation process is frictionless and quasi-static (infinitely slow thermodynamically).
7. In a nanoindentation procedure, the applied force P is proportional to the square of the indentation depth h , following Kick's Law: $P = Ch^2$ where C is a constant.
8. The AFM probe is assumed to be pyramidal, which corresponds to a C_{u} value of 1.167. This is a constant that will be used in the residual stress calculations.

Procedure

1. Each sample was indented with an AFM tip to a constant probe deflection of d_{max} throughout all trials of the experiment. The data points for the retracting portion of the force curve were saved by the proprietary AFM software in a probe deflection versus sample height (d vs. Z) plot.
2. The d versus Z values at each point were converted into P and h values using the following relations. First, Hooke’s law was applied to find the force between the probe and sample, using $k = 40 \text{ N/m}$ as the nominal spring constant of the AFM probe used in the experiment. This was also applied to convert d_{max} into its equivalent force value P_{max} .

$$\begin{aligned}
 P &= kd \\
 P_{max} &= kd_{max}
 \end{aligned}
 \tag{9.4}$$

Then, the indentation height was found by computing the probe height Z_{probe} as the reverse of the sample height and compensating for probe deflection:

$$Z_{probe} = -Z; \quad h = Z - d$$

3. The portion of the retracting force curve at maximum measured force value $(P_{max})_{meas}$ was located. If this was a point, the point’s P and h values were saved. If this was a plateau with several values of h , then only the point with the minimum h value was maintained and all points with greater values of h were discarded.
4. The point with the P value closest to $(P_{max})_{meas} - P_{max}$ was located. It height and force values were denoted $h_{normalize}$ and $P_{normalize}$, respectively.
5. The point found in step 4 was defined as the zero force and zero height point; the curve was normalized relative to the zero point by subtracting $h_{normalize}$ from every h value and $P_{normalize}$ from every P value. After normalization, any points with h and P values below zero were discarded.
6. The constant C for each curve was computed by fitting the curve to the 2nd degree polynomial $P = Ch^2$, in accordance with Kick’s Law.
7. The following values were retrieved for each fitted curve at the P_{max} point, as illustrated in 3d.
 - a. $\frac{dP}{dh}$, the initial unloading slope of the curve
 - b. h_{max} , the height of the curve
8. The area of indentation A and average contact pressure p_{avg} for each stressed curve were calculated using the following relation. This step was not necessary for the unstressed curve [10].

$$A = \left(\frac{dp}{dh} \frac{1}{c_u E^*} \right)^2
 \tag{9.5}$$

$$p_{\text{avg}} = \frac{P_{\text{max}}}{A} \quad (9.6)$$

9. Once all samples, including the unstressed sample, had undergone steps 1–7, the properties of each stressed sample curve were evaluated against the unstressed reference curve in each possible combination. In this experiment, each sample had five trials; therefore, five stressed curves evaluated against each of the five unstressed curves yielded a total of 25 analyses per sample.
 - a. First, the C polynomial coefficient of the stressed sample was compared to the corresponding C_o coefficient of the unstressed sample. If $C < C_o$, the residual stress was tensile. If $C > C_o$, the residual stress was compressive [10].
 - b. The tensile residual stress magnitude σ_H was calculated using the following relation [10]:

$$\left(\frac{h_{\text{max}}}{h_{\text{max}_o}} \right)^2 = \left(1 - \frac{\sigma_H}{p_{\text{avg}}} \right)^{-1} \quad (9.7)$$

The compressive residual stress magnitude σ_H was calculated using the following relation [10]:

$$\left(\frac{h_{\text{max}}}{h_{\text{max}_o}} \right)^2 = \left(1 + \frac{\sigma_H \sin \alpha}{p_{\text{avg}}} \right)^{-1} \quad (9.8)$$

In both relations, h_{max} corresponded to the stressed sample and h_{max_o} corresponded to the unstressed sample.

10. A positive sign is applied to the tensile residual stress values, and a negative sign to the compressive residual stress values.
11. All measured stress values were averaged for a given sample.

9.3 Results and Discussion

The constant-height trials are plotted in Fig. 9.4a, and the constant-time trials are plotted in Fig. 9.4b. The residual stress is plotted against the voltage, with separate lines for each duty cycle and pulse period combination, detailed in the legends.

For the constant-height trials, the residual stress was overall seen to increase with increasing applied voltage throughout the trials. For the constant-time trials, an overall decreasing trend was seen. The overall increasing trend for residual stress with respect to voltage for the constant-height trials suggests that higher residual stress is induced by higher current densities. The overall decreasing trend suggests

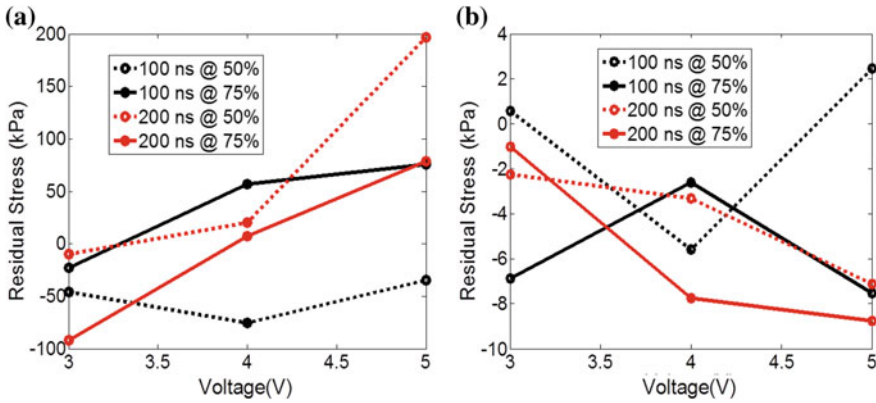


Fig. 9.4 Residual stress plots of **a** constant-height trials and **b** constant-time trials

that in the early stages of deposition at a higher voltage, a different mechanism occurs that increases the compressive stress in the part. The exceptions occurred when the pulse period was 100 ns and the duty cycle was 50% in the constant-height trials and both 50% duty cycle trials in the constant-time experiments.

Overall, for constant-height trials, which had a total deposition time of over a minute, the residual stress increase with voltage is lower in trials with a 100 ns pulse period, suggesting that it is optimal to lower the pulse period if parts need to be manufactured at higher voltages. For the constant-time trials, which lasted a shorter time, this trend did not exist. The stress ranges did not significantly vary among depositions of varying duty cycles and pulse periods. This suggests that the stresses did not develop to the full extent of the constant-height trials due to the shorter deposition time. Furthermore, lowering the duty cycle can cause the residual stress to decrease instead of increase, as seen in the data for the 100 ns pulse period 50% duty cycle trials for both constant-height and constant-time deposits, between 3 and 4 V. The opposite trend was seen for the 100 ns constant-time trial at 75% duty cycle, suggesting a different mechanism of deposition.

For the constant-height trials, increasing the applied duty cycle was seen to cause lower residual stress at a higher pulse period, while increasing the applied duty cycle was seen to cause higher residual stress at a lower pulse period. This indicates that the influence of the duty cycle on the residual stress of the deposit is dictated by the pulse period. At 4 V, for the constant-height trials, the resulting residual stress increased with increasing total pulse on time over an identical length of time. The data deviated from this relationship when 3 and 5 V were applied, suggesting a different mechanism of deposition at varying voltages.

9.4 Conclusions

According to literature, a lower current density yields a needle-like microstructure and a higher current density yields a coarser microstructure. This is correlated respectively with residual stress increasing from negative values to positive values. In the constant-height trials, this trend is clearly seen as a function of applied tool voltage, which is proportionally related to the resulting current density. As suggested in literature, this transition from negative to positive residual stress suggests that there is an optimal voltage and current density condition along this range that would yield zero residual stress [12].

The duty cycle has a different impact on the residual stress of the deposit, depending on the pulse period. At the lower pulse period, a higher duty cycle gave more positive residual stress in the deposit, suggesting a higher current density. At the higher pulse period, a higher duty cycle resulted in lower residual stress in the deposit, suggesting a lower current density. In electrochemistry, the current density always reaches a limiting value for a given set of parameters—the output residual stress may give a clue to the limiting current density occurring. Another explanation could be the fact that peak current density conditions give faster nucleation rates and a finer microstructure, which would lead to more negative residual stresses [13].

However, there is a significant deviation from any clear trends in the constant-time trials. This may be explained by the fact that higher current densities result in deposits of greater thickness variation, which then influences the resulting residual stress [12]. This would have been mitigated in the deposits that were grown to a consistent height, but not so in the constant-time deposits which could have grown to inconsistent heights. This suggests that a closed-loop control system may be preferable to an open-loop control system in order to ensure that the output ECAM parts are of a predictable residual stress.

Overall, the ECAM process holds advantages of traditional additive manufacturing, and other electroplating methods. Parts manufactured using the ECAM process exhibit residual stresses lower than traditional thermal-based additive manufacturing processes. The ECAM process also provides enhanced local control of the input parameters and therefore the output residual stress. Ideas for future work include the influence of additives in electrolyte [14], and the programmed control of plating current over time [15].

Acknowledgements Financial support provided by the National Science Foundation under Grant Nos. CMMI-1454181 and CMMI-1400800 is acknowledged.

References

1. Kruth, J.P., Froyen, L., Van Vaerenbergh, J., Mercelis, P., Rombouts, M., Lauwers, B.: Selective laser melting of iron-based powder. *J. Mater. Process. Technol.* **149**(1–3), 616–622 (2004)

2. Sundaram, M.M., Kamaraj, A.B., Kumar, V.S.: Mask-less electrochemical additive manufacturing: a feasibility study. *J. Manuf. Sci. Eng.* **137**(2), 021006 (2015)
3. Kamaraj, A.B., Sundaram, M.: A study on the effect of inter-electrode gap and pulse voltage on current density in electrochemical additive manufacturing. *J. Appl. Electrochem.* **48**(4), 463–469 (2018)
4. Bard, A.J., Huesser, O.E., Craston, D.H.: High resolution deposition and etching in polymer films. United States Patent No. 4,968,390 (1990)
5. Chan, K.C., Qu, N.S., Zhu, D.: Effect of reverse pulse current on the internal stress of electroformed nickel. *J. Mater. Process. Technol.* **63**(1–3), 819–822 (1997)
6. Basrou, S., Robert, L.: X-ray characterization of residual stresses in electroplated nickel used in LIGA technique. *Mater. Sci. Eng. A* **288**(2), 270–274 (2000)
7. Song, C., Du, L., Zhao, W., Zhu, H., Zhao, W., Wang, W.: Effectiveness of stress release geometries on reducing residual stress in electroforming metal microstructure. *J. Micromech. Microeng.* **28**(4), 045010 (2018)
8. Kume, T., Egawa, S., Yamaguchi, G., Mimura, H.: Influence of residual stress of electrodeposited layer on shape replication accuracy in Ni electroforming. *Procedia CIRP* **42**, 783–787 (2016)
9. Daryadel, S., Behroozfar, A., Morsali, S.R., Moreno, S., Baniasadi, M., Bykova, J., Bernal, R.A., Minary-Jolandan, M.: Localized pulsed electrodeposition process for three-dimensional printing of nanotwinned metallic nanostructures. *Nano Lett.* **18**(1), 208–214 (2018)
10. Suresh, S., Giannakopoulos, A.: A new method for estimating residual stresses by instrumented sharp indentation. *Acta Mater.* **46**(16), 5755–5767 (1998)
11. Li, X., Bhushan, B.: A review of nanoindentation continuous stiffness measurement technique and its applications. *Mater. Charact.* **48**(1), 11–36 (2002)
12. Kilinc, Y., Unal, U., Alaca, B.E.: Residual stress gradients in electroplated nickel thin films. *Microelectron. Eng.* **134**, 60–67 (2015)
13. Marro, J.B., Darroudi, T., Okoro, C.A., Obeng, Y.S., Richardson, K.C.: The influence of pulsed electroplating frequency and duty cycle on copper film microstructure and stress state. *Thin Solid Films* **621**, 91 (2017)
14. Lee, W., Lee, S., Kim, B., Kim, H.: Relief of residual stress of electrodeposited nickel by amine as additive in sulfamate electrolyte. *Mater. Lett.* **198**, 54–56 (2017)
15. Kao, L.C., Hsu, L.H., Brahma, S., Huang, B.C., Liu, C.C., Lo, K.Y.: Stabilized copper plating method by programmed electroplated current: accumulation of densely packed copper grains in the interconnect. *Appl. Surf. Sci.* **388**, 228–233 (2016)